Al-Aqsa University Journal - Natural Sciences Series, Volume 25, Issue 1, January 2023, pp. 68-89
ISSN 2070-3155

تقييم مؤشرات الاستشعار عن بعد الطيفية لتوصيف الجزيرة الحضرية الباردة خلال موسم الجفاف باستخدام القمر الصناعي لاند سات 8: دراسة حالة مناخية لإقليم غزة الحار والشبه جاف

د. وسام علي عيسى

قسم الجغرافيا، جامعة الأقصى، غزة – فلسطين

(تاريخ الاستلام 2022/10/25، تاريخ القبول 2022/12/21)

Evaluation of spectral indices for characterizing Urban Cool Island during the dry season from Landsat8; a hot semi-arid climate case study of the Gaza Strip.

Dr. Wissam Ali Issa

Geography Department, Al-Aqsa University, Gaza – Palestine

(Received 25/10/2022, Accepted 21/21/2022)

د. وسام عيسى – قسم الجغرافيا، جامعة الأقصى، غزة – فلسطين- E-mail address: wiesam@alaqsa.edu.ps

Evaluation of spectral indices for characterizing Urban Cool Island during the dry season from Landsat8; a hot semi-arid climate case study of the Gaza Strip.)

الملخص:

تمت دراسة العديد من مؤشرات الاستشعار عن بعد الطيفية Spectral Remote Sensing Indices بتعمق في تحديد خصائص الأنماط المكانية لظاهرة الجزيرة الحضرية الحارة Urban Heat Island (UHI) والتي تميز المناطق المناخية المعتدلة وشبه الاستوائية. ومع ذلك ، فإن تلك الدراسات كانت ولازالت قليلة في تقييم تلك المؤشرات في المناطق المناخية الحارة وشبه الجافة مثل مناطق قطاع غزة. القليل من الدراسات اوضحت بان تلك الظاهرة تتواجد بشكل معكوس في المناطق الحارة وشبه الجافة حيث تسمى بظاهرة الجزيرة الحضرية الباردة Urban Cool Island (UCI). الخصائص الطيفية المنعكسة لأغطية سطح الأرض في المناطق المناخية الحارة وشبه الجافة لها استجابة مختلفة لدرجات حرارة سطح الأرض Land Surface Temperature (LST) عن المناطق المناخية الأخرى. لذلك، فإن الهدف من هذه الورقة البحثية هو تحديد وتوصيف ظاهرة الجزيرة الحضرية الباردة باستخدام مؤشرات الاستشعار عن بعد الطيفية في فصل الصيف و هو موسم حار و شبه جاف في قطاع غزة.

أصبحت العديد من مؤشرات الاستشعار عن بعد الطيفية متاحة وتعتبر واعدة في توصيف الأنماط الطيفية والحرارية للمناطق الحضرية، حيث يمكن استخدامها لاحقًا كمدخلات للعديد من الدراسات الحضرية وتطبيقات النمذجة المناخية الحضرية. ولذلك فان أهداف هذه الدراسة هي: (1) توصيف التوزيع المكاني لوجود ظاهرة الجزر الحضرية الحارة UCI فوق اقليم قطاع غزة مثالا على الاقليم المناخي الحار و شبه الجاف; (2) تقييم ما يقرب من 21 مؤشرا طيفيا (اسماء المؤشرات الكاملة في الجدول 2) (وهي: ABEI و BAEI و BI و BRBA و BSI و BUI و DBSIو ENBI و IBI و I_Imp و MSAVI2 و NBI و NBUI و NDBI و NDSI و NDVI و SAVI و UI و VgNIR-BI و VrNIR-BIوVIBI) في توصيف النمط الحراري المكاني الحضري بناءً على سيناريوهين مختلفين للغطاء الأرضي؛ السيناريو الاول يشمل كل الغطائات معا "All" (بما في ذلك المناطق الحضرية والكثبان الرملية والمناطق العشبية والتربة القاحلة) والسيناريو الاخر يضم الغطاء الحضري فقط "Urban". حيث تم اشتقاق خرائط المؤشرات الطيفية بحجم بكسلات 30 متر و اشتقاق خرائط درجات الحرارة السطحية (LST) بحجم بكسلات 100 متر من مرئيات القمر الصناعي لاندسات 8 لصيف 2017 ومعالجتها (مسبقًا) .

من خلال هذه الدراسة, أثبتت النتائج وجود ظاهرة الجزيرة الحضرية الباردة UCI في المناطق المناخية الحارة وشبه الجافة (قطاع غزة). حيث سجلت الدراسة أعلى ارتباط مكاني (R^2) الذي تم ايجاده باستخدام معادلة البولينوميال من الدرجة الثانية ما بين درجات الحرارة (LST) والمؤشرات الطيفية (SPs) المدروسة ضمن سيناريو "ALL" هي ؛ DBSI (R^2= 0.58) ، ABEI (R^2 = 0.52)، BSI (R^2= 0.50)، و BAEI (R^2= 0.44) ، في حين أن الارتباط الاعلى ضمن سيناريو "Urban" هو: MSAVI2 (R^2= 0.50) ، P_imp (R^2= 0.40) ، ABEI (R^2= 0.33)، و NBI (R^2= 0.33).

(الكلمات المفتاحية: لاندسات 8 ؛ الجزر الحضرية الباردة (UCI)؛ درجة حرارة سطح الأرض (LST) ؛ المؤشرات الطيفية (SPs) ؛ المناخ الحار والشبه الجاف, قطاع غزة).

Abstract:

Several Spectral Remote Sensing Indices have been widely investigated for characterizing the spatial patterns of urban heat islands (UHI) phenomenon commonly found in temperate and subtropical climate regions. However, those studies were and still are few in evaluating these indicators in hot and semi-arid climatic regions such as the Gaza Strip. A few studies have shown that this phenomenon occurs in reverse in hot and semi-arid regions, where it is called the urban cool island (UCI) phenomenon. The spectral characteristics of land covers in the hot arid and semi-arid climate regions have a different response to land surface temperatures (LST) from other climatic regions. Therefore, the goal of this paper is to identify and characterize the UCI using spectral indices (SIs) during a dry season over the hot arid, and semi-arid climate area of the Gaza Strip.

SIs have become readily available and are considered promising for characterizing the spectral and thermal patterns of urban and non-urban areas, whereas the thermal spatial pattern can be used later as inputs in many urban studies and climatic modeling applications. The aims of this study are; (1) to identify the presence of the UCI phenomenon over the hot arid and semi-arid climate area of the Gaza Strip; (2) to evaluate 21 SIs (SIs' full names mentioned in table 2) including; ABEI, BAEI, BI, BRBA, BSI, BUI, DBSI, ENBI, IBI, I_imp, MSAVI2, NBI, NBUI, NDBI, NDSI, NDVI, SAVI, UI, VgNIR-BI, VrNIR-BI, and VIBI for characterizing the UCI pattern over the Gaza Strip. The spatial analysis was applied in two land cover scenarios; including the “All” classes scenario (urban, all vegetation types, bare soil, and sand), and the “urban” class. The LST (100 m) and spectral indices (30 m) are derived from Landsat 8 images of summer.

The results of this research provided the existence of the UCI phenomenon in the hot arid and semi-arid climate area of the Gaza Strip. The statistical relationship between SIs and UCI is best-described using the second-order polynomial fit, within the "All" class are the following SIs; DBSI (R^2 = 0.58), ABEI (R^2 = 0.52), BSI (R^2 = 0.50), and BAEI (R^2 = 0.44), whilst within the "urban" class are the following SIs; MSAVI2 (R^2 = 0.50), P_imp (R^2 = 0.40), ABEI (R^2 = 0.33), and NBI (R^2= 0.33).

Keywords: Landsat 8; urban cool island (UCI); land surface temperature (LST); spectral indices (SIs); arid and semi-arid climate; the Gaza Strip.

.

Evaluation of spectral indices for characterizing Urban Cool Island during the dry season from Landsat8; a hot semi-arid climate case study of the Gaza Strip.

1

. Introduction

Ongoing urbanization plays an essential role in the modification of the local climate. About 52% of the world's population now resides in urban areas, which is expected to increase to 67% in 2050 [1]. The rapid expansion of anthropogenic land cover causes an increase in urban land surface temperature (LST) leading to warming the urbanized areas more than the surrounding non-urbanized (rural) areas, which is also described as the urban heat island (UHI) effect [2]. UHIs are frequently found in temperate and sub-tropical climate areas [3-5] during the evening or nocturnal time [6]. In contrast, natural land covers (e.g., bare soil) were also found to play an essential role in reversing the urban cool island (UCI) phenomenon within dry and hot areas such as arid and semi-arid climate areas [7-10]. The dry bare soil and sand emit higher LST within the urban surroundings than in the urbanized area [3,9]. UCI has been recorded in the morning and early afternoon during fair weather and low wind speed conditions [6,11,12].

In the last years, a few studies [3,4,6-8,11-13] have been emphasizing the inversion of the UHI phenomenon (i.e., Urban Cool Island), especially in the hot arid, and semi-arid climate areas. Erbil city in Iraq [3] shows the presence of UCI as a case study of hot arid and semi-arid climates. The study indicates that densely built-up areas such as central districts of the city, green areas, and water bodies, had lower LST acting as cool islands, compared to the non-urbanized area around the city. Rasul et al. [3] found soil wetness to be the main determinant of the UCI effect, and not vegetation cover. Other cities in dry or semi-arid regions with dry surroundings reveal similar results e.g. Dubai and Abu Dhabi [14,15], Beijing [15], Okayama [16], Chang-Zhu-Tan [17], Tehran [7], Isfahan [4], Kuwait [12] which has been termed the Urban Cool Island (UCI) effect. UHI has a high heat storage capacity and low solar radiation on urban surfaces, this probably explains why the UHI phenomenon is often observed, but the UCI phenomenon is rarely observed [11]. Literature has indicated different causes of UCI, which are varied by geographic locations including; shadows effects of urban structure [12,18-20]; energy storage characteristics of urban materials [21]; aerosols contamination of urban areas [13]; the heating/cooling thermal properties of different LULC e.g. soil moisture [3,7,12, 22, 23]; sea breeze [12,24]; atmospheric boundary-layer dynamics [6,12]; and evaporative moist of urban soil compared to the dry rural soil [3,8,12,15] or dry sand zones [14]. Moreover, Gago et al. [20] explain the reversal of UHI (an urban heat sink\UCI) in the day depends on certain surface situations, which could be one or more that creates the UCI. Urban structure materials are different in terms of their internal thermal and biophysical properties (e.g., heat capacity, thermal conductivity, and inertia), which have a big importance in the control of the temperature of a body in balance with its environment [25]. Where these properties change according to the type of soil and its moisture content [26]. Dry, bare, and low-density soils have high LST because of their low thermal inertia [27, 28].

Since the early 1900s, hundreds of UHI studies of urban areas around the world have been assessed for temperate climate areas [29,30], using remote sensing spectral indices (SIs), which are frequently

used in those studies [15,31,32] to examine the relationship between UHI and Land cover (LC). However, little research has been investigating this relationship where the inverse of UHI (UCI) exists in arid and semi-arid environments [3,4]. For example, Schwarz et al. [33] studied the UHI of 263 European cities and found that differentiating cities into various thermal climate zones increased the correlation with the selected indicators. The study showed differences and instabilities of those indicators chosen for quantifying surface urban heat islands and should use several indicators in parallel for describing the surface urban heat island of a city. Erbil case study [3] a city with a semi-arid climate, NDBI, and NDVI are tested for quantifying the spatial structure of UCI in different LULC and districts to establish the key determinant factors and patterns of the spatial distribution of LST(UCI). The study shows a strong positive relationship (R^2 = 0.58) between mean LST and NDBI. Meanwhile, a negligible inverse relationship (R^2 = - 0.15) is found, between LST and NDVI. Another study in Erbil [3] examined the relationship between LST and LC using wetness, brightness, bareness, built-up, and vegetation index maps, the study found a high positive correlation with LST, while, the second important factor was the inverse correlation of wetness for determining LST. Additional study in Erbil [8] during the daytime, in summer, autumn, and winter, densely built-up areas had lower LST acting as a UCI compared to the non-urbanized area around the city. LST - NDVI relationship is affected by seasonality and strongly inverted in spring (R^2 = 0.73). Rasul et al. [8] reviewed NDVI and LST correlation in UHI studies, the study emphasized that although NDVI has been applied widely, it shows different correlations in different cities because of the seasonal changes, and soil and vegetation moisture content (irrigation might affect this relation in dry seasons). Contrary to previous studies of semi-arid cities, UCI was detected, not only in the morning but also during the afternoon [8]. Satellite capture timing in early July shows additional help for characterizing UCI because crops were largely pre-emergent to decrease the LST [8]. Gago et al. [20] shows a positive relationship between the bare soil and cultivated land with mean LST for three years of analysis. Moreover, Gago et al. [20] proposed that human activities such as urban expansion, crop rotation, poorly managed cropland, and vegetation degradation might have caused increases in bare/semi-bare soil. Because of that, LST remains practically constant along the rural-urban gradient, and the typical correlations can be reversed [20]. Yang et al. [11] reveals UCI exists in Hong Kong during the day, especially when anthropogenic heat is small or absent and the city experiences a significant daytime UCI effect. Gago et al. [20, 28] indicated that soil emissivity depends on soil moisture situations and soil density. Thus, for areas characterized by partial vegetation cover, the thermal surface properties can have a great influence on the measurement of LST through the thermal courses of conduction, convection, and radiation, the same previous study in Seville, Spain, shows a wide range of climate types (from subtropical to the Mediterranean) suggesting the role of bare soil and cultivated land in the reversal of the UHI phenomenon. A linear regression analysis shows a negative relationship of mean LST with impervious surface fraction due to the presence of shadows projected by buildings, and a positive relationship with green space fraction caused by the influence of bare soil and cultivated land that inverts the LST behavior pattern. The Tehran study [7,9] suggested the role of bare soils in the inversion of the UHI phenomenon with the urban-rural indicator.

Barren soils had low heat capacity and conductivity and heated by sunrise quickly, while urban surfaces were saving solar energy, and daytime images were not acquired at the peak of solar radiation. Haashemi et al. [7] found a large seasonal variation in the relationship between surface properties (e.g., LULC, impervious surface-IS, fractional vegetation cover-FVC, and albedo) and LST. Haashemi et al. [7] evaluated that using these relationships for UHI modeling may not be effective in the hot arid and semi-arid city, however, additional studies are required for more robust conclusions from other areas of the hot semi-arid climate. Research on the UCI effect is still in its infancy for characterizing the phenomenon in hot arid and semi-arid environments to be better quantified and understood [17,3].

Satellite sensors proved to be a very useful tool in monitoring urban areas of surveying with low-cost, archived time-series data, large-area coverage, and short revisit cycles [34]. LANDSAT satellite series provide nearly 45-year data records with a relatively high spatial resolution [35]. Satellite-derived LST (100 m) is considered adequate for depicting most of the intra-urban variations related to urban morphology [36]. Remote sensing imagery has been widely applied to study the relationship between LST-SIs in UHI\UCI studies. Researchers are using LANDSAT images to derive LST because of its proper spatial resolution for UHI\UCI [3,7,8,12,13,20], however, there are also studies using MODIS data [3,8,15,12,13,37] for better temporal resolution. Remote sensing imagery is an ideal tool for monitoring spatial land covers, especially in urban areas because of its capacity to offer timely distribution and synoptic views of land cover [38]. Landsat 8 (Table 1) has been equipped with 9 spectral bands and 2 thermal bands, which allows for more integration of land cover information in a form of individual bands or SIs. The land covers data are commonly generated using SIs and found to be useful for the characterization of UHI\UCI. Land cover shows to have a specific contribution to the LST budget. Moreover, SIs has been used to characterize different land-cover types [39]. Hence, the functional relationships between SIs and LSTs were found to be a useful basis for thermal sharpening [40] and modeling the distribution of UHI\UCI studies. SIs are used intensively for mapping urban areas, which are known to be complex areas of remote sensing investigation, due to the high variability of land-cover types and construction materials and the mixed pixel problem between LC classes [31,36] such as bare soil and built-up areas [41,35,42]. This is also more problematic in terms of selecting a proper sensor and a robust SI that can quantify/characterize both the spectral and thermal properties of the heterogeneous urban environment. SIs are considered promising to map impervious surface distributions due to their easy, parameter-free implementations [35]. Moreover, satellite sensors can record the spectral characteristics of land covers in different climate zone, it is found that dry hot climate regions such as hot and semi-arid regions have different spectral characteristics from other climatic regions [43].

Table 1. Technical characteristics of operational Landsat 8 OLI and TIRS bands

Band number	Wavelength (μ)	Resolution and band name
Band 1	0.435 – 0.451	30 m Costal/Aerosol

Band 2	0.452 – 0.512	30 m Blue
Band 3	0.533 – 0.590	30 m Green
Band 4	0.636 – 0.673	30 m Red
Band 5	0.851 – 0.879	30 m NIR
Band 6	1.566 – 1.651	30 m SWIR-1
Band 7	2.107 – 2.294	30 m SWIR-2
Band 8	0.503 – 0.676	15 m Pan
Band 9	1.363 – 1.384	30 m Cirrus
Band 10	10.60 – 11.19	100 m *TIR-1*
Band 11	11.50 – 12.51	100 m *TIR-2*

City urban structure, land cover type, and biophysical bio-thermal characteristics play an important role in characterizing the relationship between SIs – LST. The LST is a complex feature of green vegetation, water surfaces, impervious surface materials, and exposed soils [30]. Rasul [30] reviewed that, great progress has been done in surface UHI mapping of cities located in humid and vegetated (temperate) regions, whilst few studies have investigated the spatiotemporal variation of surface UHI\UCI and the effect of land use/land cover (LULC) change on LST in the hot arid and semi-arid climates. The review study [30] concluded that only some progress has been made, and models for simulating UHI\UCI are advancing only slowly. The study concluded and suggested that UHI\UCI in hot arid and semi-arid areas requires more in-depth research. Hence, the aims of this study are; (1) to identify the presence of the UCI phenomenon over the hot arid, and semi-arid climate area of the Gaza Strip; (2) to evaluate 21 SIs including; ABEI, BAEI, BI, BRBA, BSI, BUI, DBSI, ENBI, IBI, I_imp, MSAVI2, NBI, NBUI, NDBI, NDSI, NDVI, SAVI, UI, VgNIR-BI, VrNIR-BI, and VIBI for characterizing the UCI pattern over the Gaza Strip. The spatial analysis was applied in two land cover scenarios; including the “All” classes scenario (urban, dunes, vegetation, bare soil, and urban class), and the “urban” class.

2. Study area

The Gaza Strip (Figure. 1) is bounded by longitudes 616140 and 648576 East and latitudes 3455040 and 3496078 North, with an approximate area of 365 km^2 and ≈ 2.1 million inhabitants [47] resulting in producing one of the highest population densities around the world (≈ 5770 p/km^2). The Gaza Strip is situated in the eastern part of the Mediterranean Sea with 40 km along the seashore. Regionally, the Gaza Strip is located in the northern part of the Sinai desert as well as the western part of the Negev desert. The rainfall in the Gaza Strip gradually decreases from the north (400 mm) to the south (200 mm), and most of the rainfall occurs in the period from October to March, with the rest of the year being dry [44]. Land surface elevations is varying from mean sea level up to 110 meters. The soil in the Gaza Strip is composed mainly of three types, sand, clay, and loess. In the last decades, Gaza Strip exhibits large variations in its physical environment and population density. High demographic density triggers the rapid change in land cover. The Gaza Strip is a part of the Palestinian coastal plain located in a hot arid and semi-arid climate (type” BSh”). The land-covers map (LC) of the Gaza Strip is available from Essa and Lhissou [45]. LC map (Figure. 2) shows the high variability of the urban landscape pattern and

its heterogeneity covers an area of about ~43.5 km^2, with higher densities occurring in the urban core and lower densities in the periphery with bushes and trees. The wide range of LST values and varieties in LC classes within the Gaza Strip makes the area an adequate case to evaluate UHI/UCI existence and to calculate many SIs for characterizing the LST over the urban areas of the Gaza Strip.

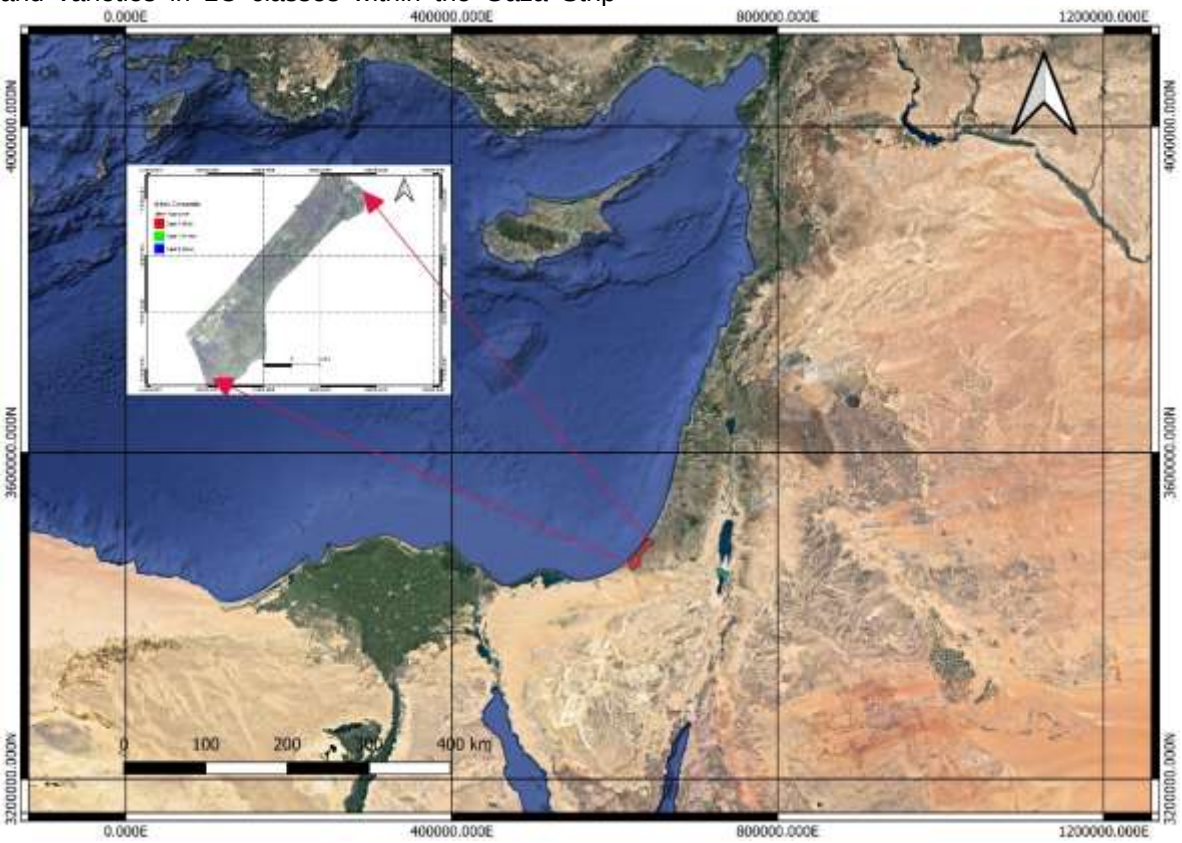

Figure 1. Study area map of the "Gaza Strip" indicating the local and regional location. The regional map was prepared using QuickMapServices Plugin in QGIS based on google satellite image background, while, the local map which is the Urban Composite Map (the red band 7, the green band 6, and the blue band 4) was prepared using the Semi-Automatic Classification Plugin [73]

3. Data and Methods

3.1. Landsat 8\LST retrieval

In this study, a Landsat 8 image was acquired on June 16, 2017 (05.50 pm). The L8 image dataset consists of two onboard sensors; 1) - The Operational Land Imager (OLI), and 2) - Thermal Infrared Sensor (TIRS), which launched in February 2013. Landsat satellites image the entire Earth every 16 days in an 8-day offset and collect up to 740 scenes per day. The OLI offers several enhancements from previous Landsat instruments, including the addition of two new spectral bands: a deep blue visible channel (Band 1) and a new infrared channel (Band 9). Two thermal infrared bands (TIRS) capture data at 100 m resolution. They are geo-registered and delivered with a 30 m spatial resolution. The land cover and land surface characteristics data for this study were produced using the surface reflectance algorithm (L8SR) for Landsat 8. The TIRS data was used to extract

daytime LST. The Landsat 8 data are available for download from the EarthExplorer USGS website (https://earthexplorer.usgs.gov). The method for retrieving the LST was carried-out using the Semi-Automatic Classification Plugin (SCP) [46], which allows the use of the free-open-source software QGIS as remote sensing software. With this plugin, temperatures are retrieved automatically from the metadata of the image acquired by the Landsat-8 satellite sensor. Mallick et al. [47] provide the emissivity (e) values of various land cover types.

3.2. Spectral Indices (SIs) retrieval

The multispectral bands of Landsat 8 (L8\OLI) image used for calculating 21 SIs are mentioned in Table. 2. The SIs that integrates LST data are not used in this application because there is no logic in drawing a correlation between LST images and indices that have the same LST data. It is also supposed that thermal data are not present. Because of that, only the spectral bands-based SIs are considered for our evaluation. The indices indicated in previous studies are based on their use to map; urban, vegetation, and bare soil land covers. L8/LST and SIs were aggregated through the spatial averaging to images with a resolution of 100 m and will refer to as “observed images”. The functional relationships between those SIs and LST were found in the literature to be a useful basis for modeling/characterizing the spatial distribution of UHI/UCI.

Table 2. 21 remote sensing spectral indices (SIs) used for statistical correlation with the Landsat 8\land surface temperature (LST) including; symbol, name, description, and reference.

Index ID	Index Name	Description	Reference
ABEI	Automated Built-Up Extraction Index	$0.312\,\rho Costal + 0.513\,\rho Blue - 0.086\,\rho Green - 0.441\,\rho Red + 0.052\,\rho NIR - 0.198\,\rho SWIR1 + 0.278\,\rho SWIR$	[69]
BAEI	Built-up Area Extraction Index	$\frac{\rho RED + 0.3}{\rho Green + \rho SWIR1}$	[48]
BI	Bare Soil Index	$BI = \rho RED + \rho SWIR1 - \rho NIR$	[43, 32]
BRBA	Band Ratio for Built-Up Area	$\frac{\rho RED}{\rho SWIR1}$	[49]
BSI	Bare Soil Index	$\frac{(\rho SWIR1 + \rho RED) - (\rho NIR + \rho BLUE)}{(\rho SWIR1 + \rho RED) + (\rho NIR + \rho BLUE)}$	[50]
BUI	Built-Up Index	$NDBI - NDVI$	[51]
DBSI	Dry Bare-Soil Index	$\frac{\rho SWIR1 - \rho Green}{\rho SWIR1 + \rho Green}$ - NDVI	[43]
ENBI	Enhancement Built-Up Index	$NDWI - FVC$	[52]
IBI	Index-Based Built-Up Index	$\frac{(NDBI - (SAVI + MNDWI))/2}{(NDBI + (SAVI + MNDWI))/2}$	[53]
P_Imp	Impervious Fraction	$P\_imp = 1 - P_v$, $P_v = \frac{(NDVI) - (NDVI)_s}{(NDVI)_g + (NDVI)_s}$	[54]
MSAVI2	Modified Soil-Adjusted	$\frac{2 \times \rho NIR + 1 - \sqrt{(2 \times \rho NIR + 1)^2 - 8(\rho NIR - \rho RED)}}{2}$	[55]

NBI	Vegetation Index New Built-Up Index	$\frac{\rho RED \ x \ \rho SWIR1}{\rho NIR}$	[48,56]
NBUI	New Built-Up Index	$EBBI - SAVI - MNDWI$	[57, 57]
NDBI	Normalized Difference Built-Up Index	$\frac{\rho SWIR - \rho NIR}{\rho SWIR + \rho NIR}$	[58]
NDSI	Normalized Difference Soil Index	$\frac{\rho NIR - \rho RED}{\rho NIR + \rho RED}$	[59]
NDVI	Normalized Difference Vegetation Index	$\frac{\rho NIR - \rho RED}{\rho NIR + \rho RED}$	[60]
SAVI	Soil Adjusted VI	$\frac{(\rho NIR - \rho RED)}{(\rho NIR + \rho RED + 1)} \times 1$	[61]
UI	Urban Index	$\frac{[\rho SWIR2 - \rho NIR]}{[\rho SWIR2 - \rho NIR]}$	[62]
VgNIR-BI	Visible Based Indices	$\frac{\rho Green - \rho NIR}{\rho Green + \rho NIR}$	[63]
VIBI	Vegetation Index Built-Up Index	$\frac{\left(\frac{\rho NIR - \rho RED}{\rho NIR + \rho RED}\right)}{\left(\frac{\rho NIR - \rho RED}{\rho NIR + \rho RED}\right) + \left(\frac{\rho SWIR1 - \rho NIR}{\rho SWIR1 + \rho NIR}\right)}$	[64]
VrNIR-BI	Visible Based Indices	$\frac{\rho RED - \rho NIR}{\rho RED + \rho NIR}$	[63]

3.3.Land-Cover map

From the multispectral bands, eight classes of land-cover maps were derived (Figure. 2) including built-up, sand, bare soil, crops, trees, shrubs, greenhouses, and wastewater. The applied classification technique is the support vector machine (SVM) method, a supervised classification method of the artificial neural network developed by Kohonen [65]. The advantage of using the SVM method approach is that mixed pixels, which occur in medium-resolution satellite data of urban areas, can be more easily identified and assigned to a separate class. This is necessary to resolve the mixed-pixels problem such as bare soil with impervious surfaces. Later, the land cover classes were grouped into two land cover scenarios for this study; 1) the “urban” class; and the “ALL” class (all classes without the wastewater).

3.4.Statistical analysis

The SIs in table (2) has been calculated at 30 m resolution and are aggregated by average to 100 m resolution image to overlap the Landsat\LST (100 m) using the nearest neighborhood resampling method. Masks of the SIs per two land-cover scenarios; 1) the “urban” class; 2) the sum of all class “All” (without the wastewater class), were prepared in separate maps (21 indices X 2 masks = 42 maps). The second-order Polynomial fit was selected after experimental tests because it shows a higher correlation between the LST maps and corresponding SIs maps. Figure. (3) Summarizes the procedure of the statistical correlation analysis.

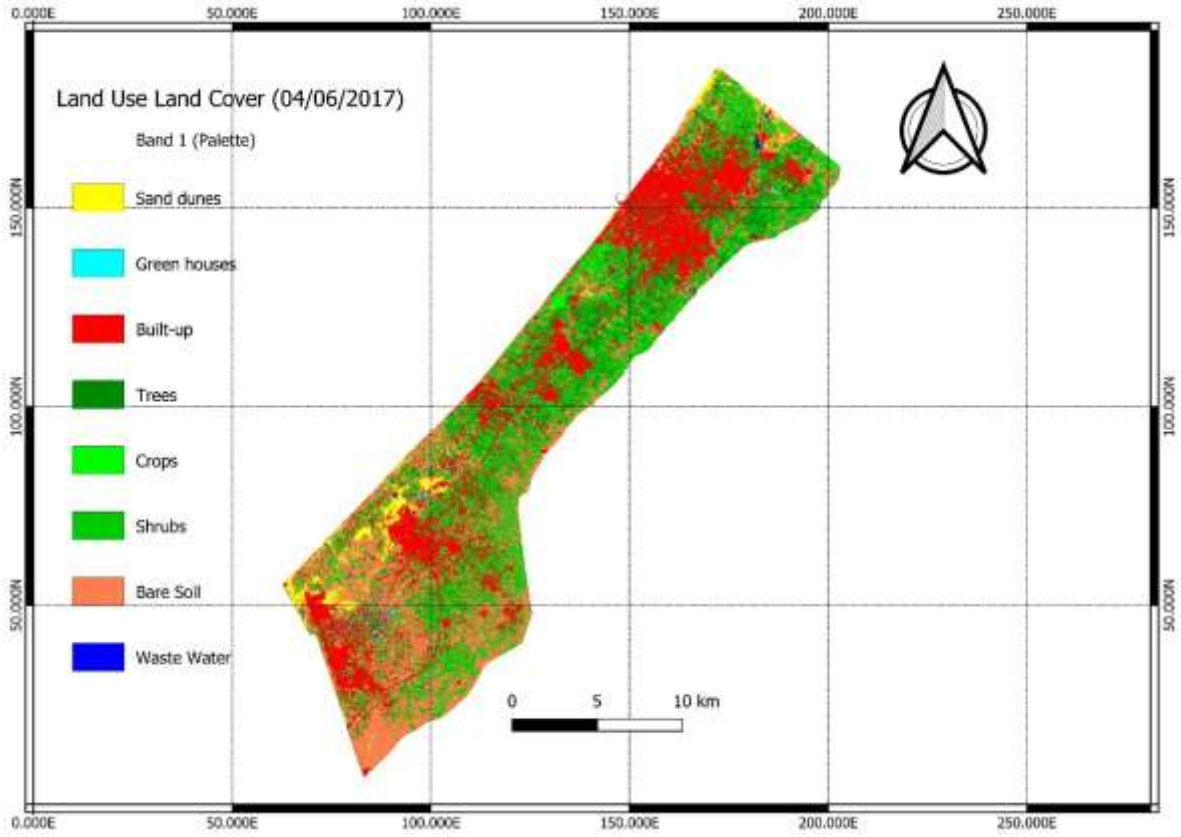

Figure 2. Land-use/Land-cover classification map of the Gaza Strip (June 2017) indicating 8 land covers, using the support vector machine (SVM) method (adapted from Essa and Lhissou. [45]).

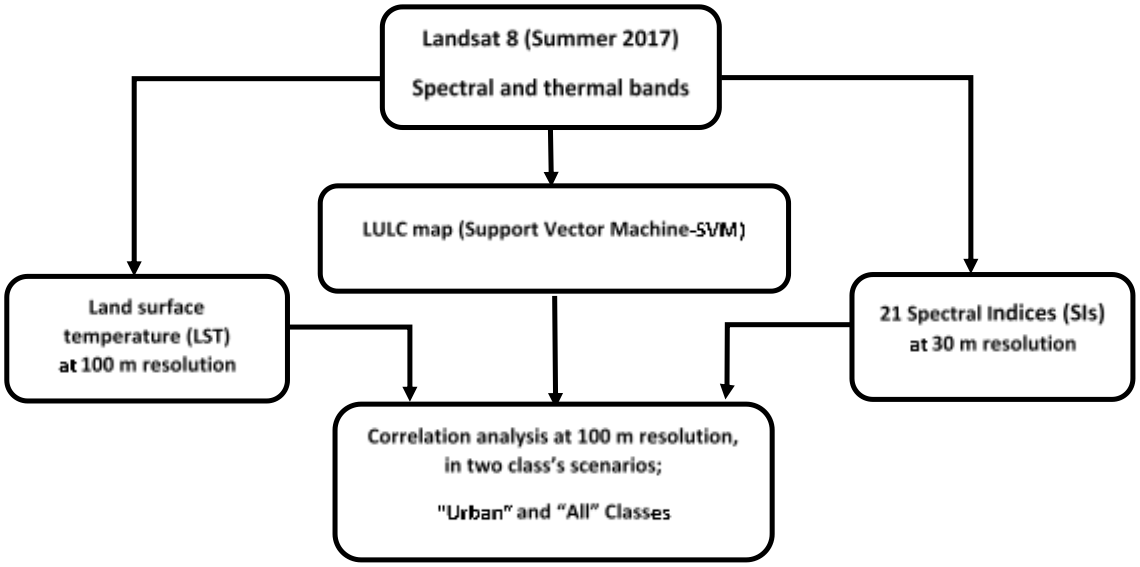

Figure 3. Flowchart showing the procedure for the correlation analysis to evaluate 21 spectral indices for quantifying land surface temperature (LST).

4. Results and discussion

4.1. Land surface temperature per land-use type

Figure. 4 presents for each land-cover type the mean surface temperature and standard deviation at 30 m resolution. The mean surface temperature for the different classes is; Wastewater (33.6 °C), trees (34.8 °C), urban (35.3 °C), crops (35.4 °C), greenhouses (36.0 °C), shrubs (37.0 °C), and (37.5 °C), bare soil (38.8 °C), and All classes, expect urban and wastewater (37.4 °C). The range between maximum and minimum temperature for each class follows the order; greenhouses (11.0 °C), sand (11.6 °C), urban (13.1 °C), all (not urban) (13.4 °C), crops (14.1 °C), shrubs (14.2 °C), bare soil (14.4 °C), trees (14.9 °C), and wastewater (15.3 °C), which shows that the greenhouses and sand classes have more uniform temperatures than vegetated areas (crops, shrubs, bare soil, and trees) and wastewater. Bare soil and sand have the highest temperatures among all classes, which agrees with other studies in the hot arid, and semi-arid areas of the Gaza Strip [3,7,9,20], which proves the existence of UCI in the Gaza Strip (hot arid, and semi-arid climate). Bare soils and sand have a critical role in the inversion of the UHI phenomenon to the UCI because of their low heat capacity and conductivity and heated by sunrise quickly, while urban surfaces were saving solar energy [7,9]. The acquired Landsat image was on June 16, 2017 (05.50 pm) for this study, which is not the peak of solar radiation. Resultantly, it is expected that those differences in temperatures be higher in value in earlier hours.

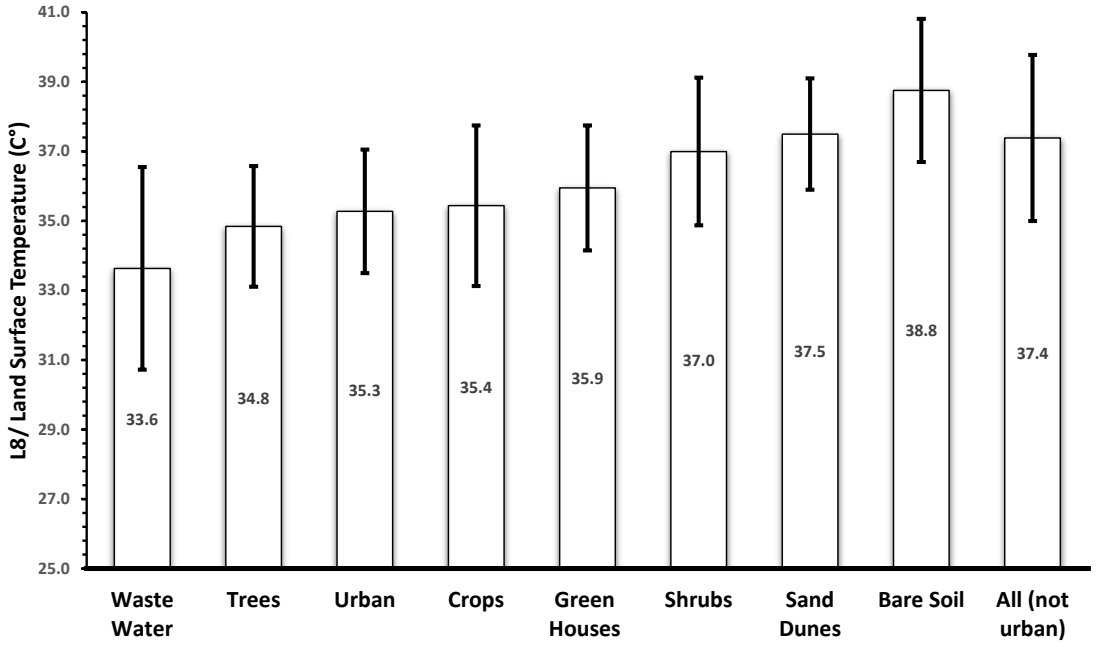

Figure 4. Land surface temperatures (mean and standard deviation) per land-cover class.

4.2. Relationship between SIs and L8\LST

The relationships between LST and the SIs were investigated in two class scenarios; 1) the "urban" class (Fig. 5), and 2) the "All" class (Fig. 6). SIs were resampled to 100 m resolution by averaging to overlay with LST image. In the “urban” class (Fig. 5), results show the correlation (R^2), which reflects

the robustness of SIs to estimate LST. Those following SIs are found to be most successfully characterizing the mixed land cover by identifying its spectral reflectance from the observed Landsat 8 LST (100 m). The R^2 are shown in descending order; the MSAVI2 (R^2 = 0.50), P_imp (R^2 = 0.40), BAEI (R^2= 0.33), NBI (R^2 = 0.33), and ABEI (R^2 = 0.31), etc. Based on the correlation of indices with LST, the LST is much more sensitive to SIs than the multispectral bands of Landsat 8. The modified soil-adjusted vegetation index (MSAVI2) shows the highest correlation with LST, which proposes that MSAVI2 accounts for most of the variation in LST across the urban class (UCI). Even though the other SIs show a lower correlation with LST, they possess valuable information for estimating UCI. The integration of those SIs using multiple linear regression analysis may help for a better estimation of the UCI. The SIs equations in the table (2) explain the robustness of the spectral bands that involve different land covers such as the built-up area (P_imp, ABEI, NBI, BAEI) and the bare soil (MSAVI2, BSI, DBSI) for estimating the UCI.

MSAVI2 shows to have the highest correlation with LST, bare soil is found dominant in the hot arid and semi-arid areas and strongly modifying the LST within the urban fabric, it is proposed that the unattached soil grains characteristics of bare and sandy soil plays additional contribution in the quick release of heat during sun radiance. The soil is heavily exposed to human activities within the Gaza Strip because it is one of the highest demographic populations (≈ 5770p/ km^2) around the world. MSAVI2 was developed by Qi et al. [66] and found successfully represents vegetation for urban areas, due to its benefit over NDVI when applied especially where plant cover has been less. MSAVI2 can perform well in the urban area even with a minimum plant cover of 15 %, whereas for NDVI the minimum plant cover required should be above 30 % [66]. A study by Bhatt et al. [67] emphasized the benefits of using MSAVI2 as compared with NDVI and MNDWI and other indices for mapping land covers in highly urbanized areas. Impervious surface area (P_imp) [54] constitutes the fraction of a pixel for which the surface can neither evaporate water nor permit rainwater to penetrate. P_imp shows the second highest correlation with LST. SIs are designed to highlight only one land cover type (e.g. vegetation and built-up area, etc.), and confusion among other land cover types, in particular impervious surfaces and bare soil, have not been successfully addressed [35,41-43], Built-up Area Extraction Index (BAEI) was proposed Bouzekri et al. [48] for highlighting built-up areas in the Landsat-8 image. In addition to using spectral channels, arithmetic constant (0.3) is also introduced to facilitate the extraction of the built-up area. This study also emphasizes the BAEI to be better than the Normalized Difference Built-up Index (NDBI) for highlighting built-up areas in the image and having a high correlation with LST. In BAEI, dense built-up areas come up very clearly [32]. The New Built-up (NBI) is proposed by [68] based on the characteristics DNs of band 3 (Red) in bare ground areas which are generally larger than those built-up areas. Higher values of the NBI would indicate a greater possibility of bare ground areas in the image [48]. The Automated Built-Up Extraction Index (ABEI) demonstrated its effectiveness to extract built-up areas from other land covers even in bare soil and sandy areas where other indices experience major challenges especially for bare and sandy areas is not optimal [69]. This study confirms that ABEI successfully can better characterize LST than other indices (DBSI, BAEI, NDBI, and BSI) in the hot arid and semi-arid regions with mixed LULC such as when the bare soil and the sandy soil are

mixed with the built-up areas. ABEI shows to perform better than simple techniques of a two-band index and single-band thresholding, which may not accurately evaluate built-up pixel's intensity, particularly in scenes where built-up bright surfaces are seen [69].

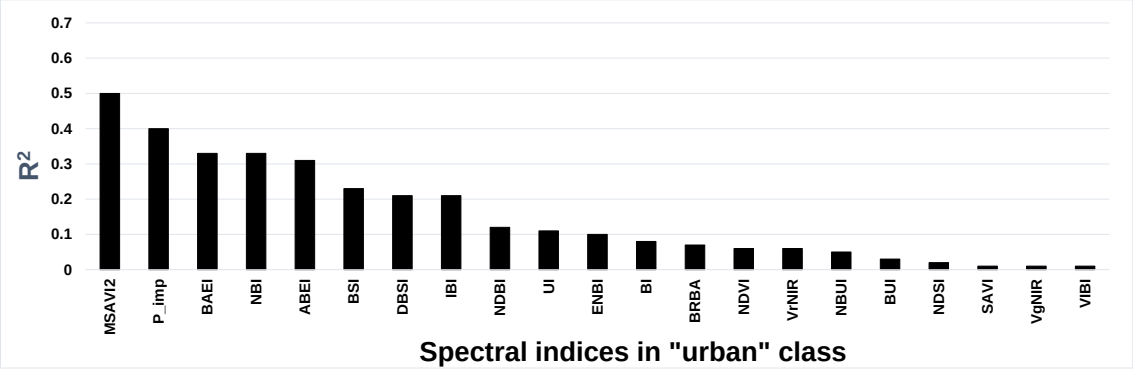

Figure 5. Correlation coefficients (R^2 - descending order) in the “urban” class for the relationship between the indices (for abbreviations see Table 2) and Landsat 8/land surface temperature at 100 m resolution.

In the class "All" (Fig. 6), correlation (R^2) is shown in descending order to follow; DBSI (R^2 = 0.58), ABEI (R^2 = 0.52), BSI (R^2 = 0.50), BAEI (R^2 = 0.44), NDBI (R^2 = 0.40), etc. DBSI is a newly proposed index by Rasul et al. [43] to map built-up and bare areas in dry climates from Landsat 8 in the city of Erbil, Iraq. A threshold of DBSI to extract built-up and bare-soil may vary based on the study site, Erbil shows a threshold of 0.26 and higher (DBSI) to delineate bare soil, and areas with lower values were delineated as other classes. DBSI can be used reliably for differentiating constructed and bare land from other land use classes in the hot arid and semi-arid climates [43], in our study area DBSI shows applicable also to characterize LST in mixed LULC classes ("ALL" class) by being the highest among other SIs to characterize LSTs. This study confirms also that ABEI successfully can also characterize LST when mixed LULC such as the bare soil with the built-up areas in the hot arid semi-arid regions. ABEI shows to perform better than simple two bands ratio SIs. This study also confirms that the proposed index can differentiate the thermal characteristics of all mixed land covers (class “All”), which is emphasized by the high correlation between the ABEI and the UCI in class “All”. Bare soil index (BSI) [50] shows similar R^2 as ABEI to characterize the UCI. BSI was found useful to map vegetation by stratifying the vegetation densities with a different background including bare soil [70]. BAEI [48] shows to highlighting built-up areas and show a higher correlation with LST, it shows the robustness to estimate also UCI on a mixed land cover environment (class “All”) in the hot arid and semi-arid climate areas. BAEI shows a higher correlation than NDBI with the UCI. NDBI was proposed in 2003 as a method to maps built-up areas automatically for Nanjing city [39] and applied by [69] in Iranian and European cities. NDBI index was able to distinguish between built-up and vegetated or green and wet surroundings for the city of Nanjing, however, NDBI was not successful in distinguishing between built-up and other land covers such as bare and dry soil that surround the city, due to the overlapping spectral reflectance for these land cover types [69]. Generally, NDBI is

more efficient in places where the NDVI value is greater than 0 [58].

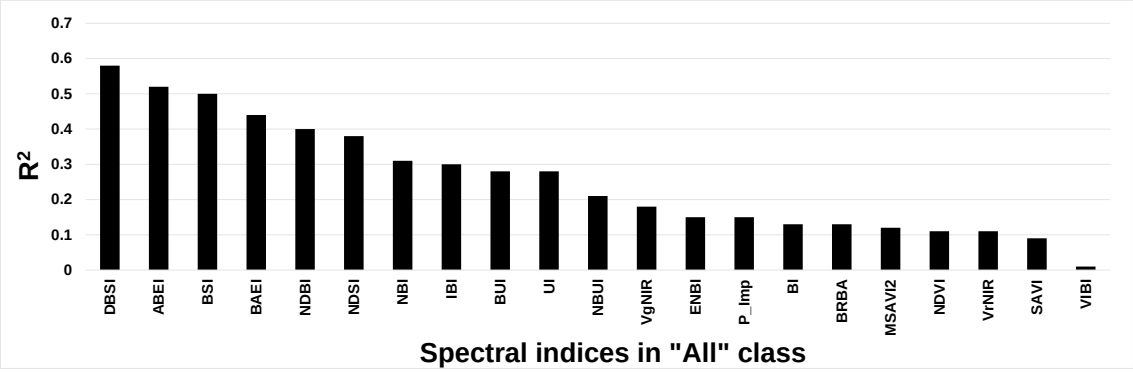

Figure 6. Correlation coefficients (R^2 - descending order) in the "All" class for the relationship between the indices (for abbreviations see Table 2) and Landsat 8/land surface temperature at 100 m resolution.

To conclude, we can propose that bare soil land cover has high contribution to estimate the UCI than a built-up. This conclusion was clear from the regression analysis with LST, as MSAVI2 and DBSI show to have the highest correlation with the LST (UCI) in class "urban" and class "All" respectively. However, other indices show a good correlation with UCI, which are still possessing valuable information for un-mixing the UCI. Future studies are supposed to integrate those indices using multiple linear regression analysis for better estimation and un-mixing the UCI based on different land cover classes.

Scatterplots analysis for the two scenarios "urban" and "All". For the urban class, the scatterplots and the second-order polynomial fit of the SIs versus L8\LST are shown in figure (7). MSAVI2 (Fig. 7a) and P_imp (Fig. 7b) shows similar show a wide range of LST values, especially around the index middle values, because the built-up materials have a wide range of temperatures. Moreover, the bare soil openings are dominant in residential areas (e.g., Bare soil paths), which can be described as a complementary part of the built-up area at the pixel level. Resultantly, the mixture of the bare soil, sandy soil, and the urban structure features have varied physical thermal properties that cause a wide range of LST. Because of that, the lower LST values are shown along with the index ranges due to the cooling and moderating the effect of built-up structure shading. Both indices show lower temperatures at both scatterplots tails, the minimum index tail shows the green part of the city with lower temperatures, while the maximum index tail shows the shading effects within the concentrated built-up part of the city, where urban shade significantly decreasing the LST. Moreover, Own et al. [71] developed a new approach based on satellite remote sensing data when it is forming a triangular-shaped envelope of pixels in urban areas like what we have in those both indices MSAVI2 and P_imp, when bare soil experience a wider variation in surface radiant temperature than densely vegetated locations in the urban area, later referred to as the "triangle method". The surface radiant temperature response along the abscissa is a function of varying vegetation cover and surface soil water content (which can be defined as a surface moisture availability).

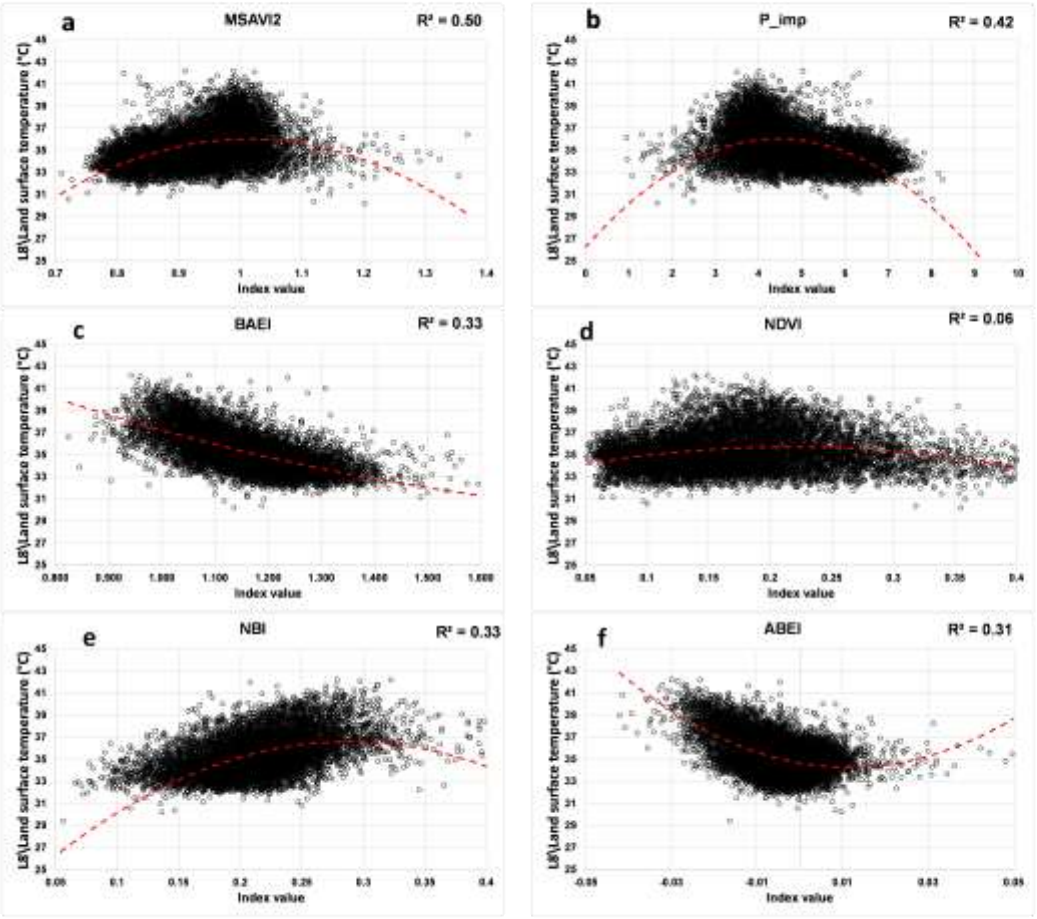

Figure 7. Scatterplots of spectral indices versus observed Landsat 8\land surface temperature for the "urban" class at 100 m resolution, using the second order polynomial fitting model.

The Built-up Area Extraction Index - BAEI (Fig. 7c) and ABEI (Fig. 7f), show a similar curve fit. When the value of both indices increases, pixels show lower temperatures, especially within the concentrated built-up part of the city, where urban shade significantly decreases the LST. A wider LST range is shown along the fitting line because built-up materials have varied physical thermal properties as described before, however, the scatters show a lower temperature range at the highest index values, due to the cooling effects of built-up areas by the shading. Comparing the NDVI scatterplot (Fig. 7d), NDVI shows no correlation, however, higher NDVI shows a lower LST value, where the possibility is related to vegetated pixels in the urban class which decrease LST values. The NBI index proposed by [32] is based on the characteristics DNs of band 3 (Red) in bare ground areas which are generally larger than those in built-up areas. Higher values of the NBI would indicate a greater possibility of bare ground areas in the image [48], and higher values of the NBI also indicate higher LST values.

Figure (8) shows the scatterplots of SIs versus L8\LST for the "All" class. SIs including; Dry Bare-Soil Index (DBSI), Bare Soil Index (BSI), and Normalized Difference Built-Up Index (NDBI) (Fig. 8a+c+f) are showing similar scatters. The lower tail of SIs shows scattered shows lower temperatures, where the added vegetation cover that has a lower LST value to the regression analysis causes the cooling and moderating effect. However, when the SIs values increase, temperatures increase as well due to the integration of a wide space of bare soil and sandy soil land cover into the regression analysis that has a higher LST value causing the hooting effect. ABEI and BAEI (Fig. 8b+e respectively) show also similar scatterplots, LST has a wider range along the fitting line due to the variable temperature range introduced by the different land covers and their thermal properties. The lower index value tail shows the higher temperatures of the bare soil and sandy soil, while the higher index value tail shows the lower temperatures of vegetated areas and the shaded built-up areas. Moreover, the NDVI scatterplot (Fig. 8d) shows a better correlation (R^2 =0.11) than the urban class (R^2 =0.07) which is shown in Figure. (7d), because of integrating the vegetation classes into the regression analysis.

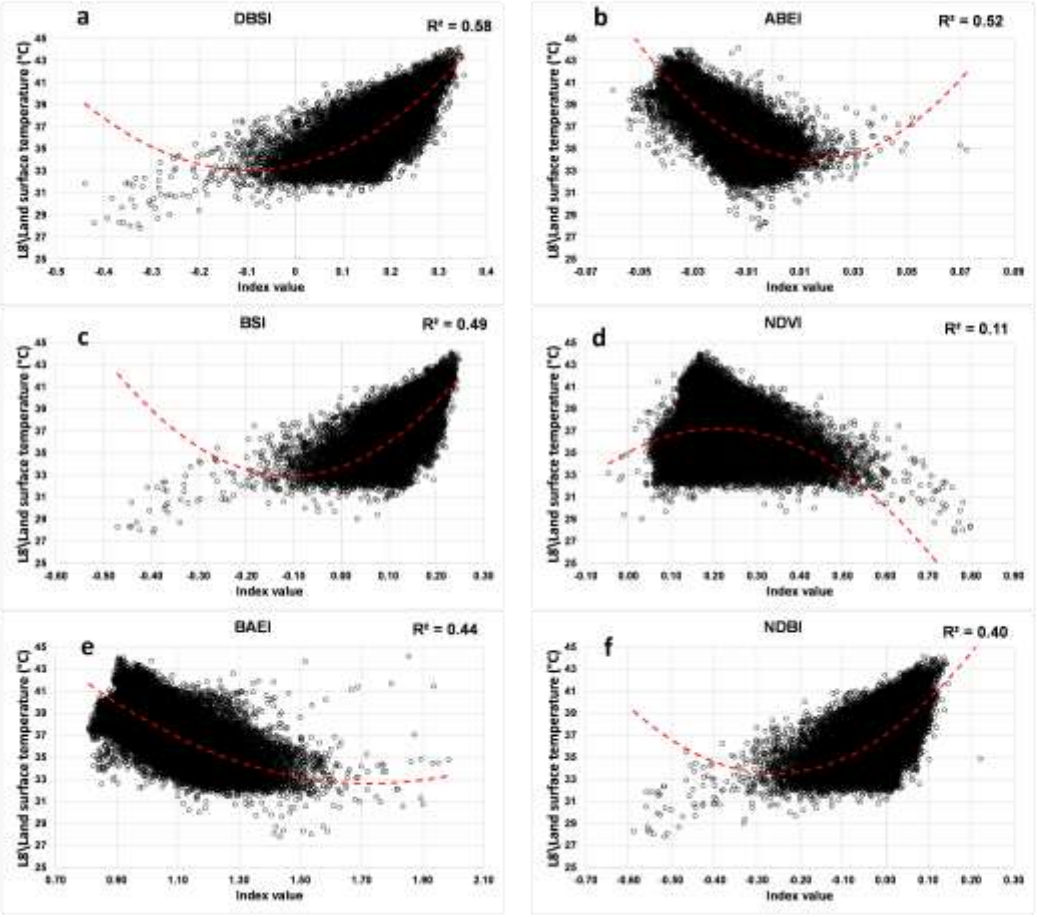

Figure 8. Scatterplots of spectral indices vs observed Landsat 8\land surface temperature for the "All" class at 100 m resolution, using the second order polynomial fitting model.

4.3. SIs-LST regression Models

The slope, intercept, and coefficient of determination (R^2) for the second-order polynomial regression of best SIs are shown by the equations (1-10).

For the "All" class, the models shown for; DBSI, ABEI, BSI, BAEI, and NDBI are shown in equations 1-5 respectively, and for the "urban" class, the models MSAVI2, P_imp, BAEI, NBI, and ABEI are shown in the equations 6-10 respectively. The high correlation analysis justifies its use for defining models for quantifying/estimating LST (UCI) [72]. The high R^2 reveals the robustness of those models to account for quantifying the variation in LST. However, other models still possess valuable information for estimating LST (UCI). It is suggestible that integrating those one-factor models into a multiple-fact regression model (multi-regression analysis), helps in a better estimation of the UCI, which will be investigated in the future for applications related to thermal downscaling.

$$LST_{all\ classes} = 51.116\,(DBSI)^2 + 9.747\,(DBSI) + 33.535 \quad R^2\ (0.58) \quad (1)$$

$$LST_{all\ classes} = 2444.4\,(ABEI)^2 - 75.408\,(ABEI) + 34.627 \quad R^2\ (0.52) \quad (2)$$

$$LST_{all\ classes} = 70.625\,(BSI)^2 + 15.18\,(BSI) + 33.75 \quad R^2\ (0.50) \quad (3)$$

$$LST_{all\ classes} = 10.669\,(BAEI)^2 - 36.876\,(BAEI) + 64.486 \quad R^2\ (0.44) \quad (4)$$

$$LST_{all\ classes} = 52.258\,(NDBI)^2 + 26.998\,(NDBI) + 37.029 \quad R^2\ (0.40) \quad (5)$$

$$LST_{Urban} = -53.541\,(MSAVI2)^2 + 108.45\,(MSAVI2) - 18.891 \quad R^2\ (0.50) \quad (6)$$

$$LST_{Urban} = -0.4936(P\_imp)^2 + 4.3977\,(P\_imp) + 26.25 \quad R^2\ (0.40) \quad (7)$$

$$LST_{Urban} = 5.7215\,(BAEI)^2 - 24.743\,(BAEI) + 56.248 \quad R^2\ (0.33) \quad (8)$$

$$LST_{Urban} = -181.82(NBI)^2 + 104.86\,(NBI) + 21.49 \quad R^2\ (0.33) \quad (9)$$

$$LST_{Urban} = 2984.82(ABEI)^2 - 68.465\,(ABEI) + 34.652 \quad R^2\ (0.31) \quad (10)$$

5. Conclusion

In this study, we reported and explained the existence of the day UCI phenomenon within the hot arid, and semi-arid climate area of the Gaza Strip, even though the urban areas are characterized by a low-rise compact city.

The study confirms other previous studies on UCI [e.g., 3]. UCI was revealed from the mean temperature between land cover classes. The

urbanized areas have been found with lower temperatures of -3.5 °C and -2.2 °C than the city surrounding natural land covers of bare soil and sandy soil respectively.

21 Spectral Indices (SIs) have been evaluated for characterizing LST (UCI). A second-order polynomial relationship shows to be the best fit to characterize the relationship between spectral indices and LST in urban and non-urban areas within the study area. Although built-up and bare soil indices have been found useful to characterize UCI, bare soil indices have been shown to possess the highest correlation than built-up indices. The modified soil-adjusted vegetation index (MSAVI2) has shown the highest correlation with LST within the urban class (R^2 = 0.50), while the dry bare-soil index (DBSI) shows to have the highest correlation within the "All" class (R^2 = 0.58).

This research on UCI can help city planners in the thermal comfort planning of the city, by adapting construction regulations that increase the shaded areas. Moreover, it helps in planning non-urban areas by increasing the vegetated cover, increasing soil wetness, or adapting urbanization expansion policies.

Unlike tropical and cold cities that experience the urban heat island effect, the Gaza Strip, with its hot arid, and semi-arid climate type, experienced the urban cool island effect. UCI has resulted from the surrounding bare soils with high surface temperature enclosing the built-up areas, however, the sea breeze cooling might have effects which is needed to be investigated in future research.

The Landsat 8\LST image was acquired on June summertime 16, 2017 (05.50 pm) in this study, which is not the daily peak of solar radiation. However, it is expected that higher UCI intensity in earlier hours.

Acknowledgments: The research was supported by Royal Geographical Society RGS – IBG Small Research Grants.

References

United Nations, Department of Economic and Social Affairs, Population Division 2014 World Urbanization Prospects: The 2014 Revision, Highlights (ST/ESA/SER.A/352) (http://esa.un.org/unpd/wup/highlights/wup2014-highlights.pdf) (accessed on 22 November **2020**)

Voogt, J.A.; Oke, T.R. Thermal remote sensing of urban climates. *Remote Sens. Environ*. **2003**, 86, 370–384.

Rasul, A.; Balzter, H.; Smith C. Spatial variation of the daytime Surface Urban Cool Island during the dry season in Erbil, Iraqi Kurdistan, from Landsat 8. *Urban Clim.* **2015**, 14(2), 176-186, https://doi.org/10.1016/j.uclim.2015.09.001.

M. Reisi.; M. A. Nadoushan.; L. Aye. Remote sensing for urban heat and cool islands evaluation in semi-arid areas. *Global J. Environ. Sci. Manage*. **2019**, 5(3): 319-330, DOI: 10.22034/gjesm.2019.03.05

Cui, Y. Y.; De Foy, B., (2012). Seasonal variations of the urban heat island at the surface and the near-surface and reductions due to urban vegetation in Mexico City. *J. Appl. Meteorol. Climatol*. **2012**, 51(5): 855-868 (14 pages).

Theeuwes, N.; Steeneveld, G.; Ronda, R.; Rotach, M.; Holtslag, A. Cool city mornings by urban heat. *Environ. Res. Lett.* **2015**, 10, 11, http://dx.doi.org/10.1088/1748-9326/10/11/114022

Haashemi, S.; Weng, Q.; Darvishi, A.; Alavipanah, S.K. Seasonal Variations of the Surface Urban Heat Island in a Semi-Arid City. *Remote Sens*. **2016**, 8, 352-856. https://doi.org/10.3390/rs8040352.

Rasul, A.; Balzter, H.; Smith, C. Diurnal and Seasonal Variation of Surface Urban Cool and Heat Islands in the Semi-Arid City of Erbil, Iraq. *Clim.* **2016**, 4, 42.

Guoyin, C.; Mingyi, D. Relationship between thermal inertia and urban heat sink in Beijing derived from satellite images. *JURSE Proceedings* of the **2009**, Shanghai, China, 20–22 May 2009.

Shigeta, Y.; Ohashi, Y.; Tsukamoto, O. Urban Cool Island in daytime-analysis by using thermal image and air

temperature measurements. *ICUC-7 Proceedings*, **2011**, Yokohama, Japan, 29 June–3 July 2011.

Yang, X.; Li, Y.; Luo, Z.; Chan, P.W. The urban cool island phenomenon in a high-rise high-density city and its mechanisms. *Int. J. Climatol.* **2017**, 37: 890-904. https://doi.org/10.1002/joc.4747

Alahmad, B.; Tomasso, L.; Al-Hemoud, A.; James, P.; Koutrakis, P. Spatial Distribution of Land Surface Temperatures in Kuwait: Urban Heat and Cool Islands. *Int. J. Environ. Res. Public Health* **2020**, 17(9), 2993; https://doi.org/10.3390/ijerph17092993

Bala, B.; Prasad, R.; Yadav, V.; Sharma, J. SPATIAL VARIATION OF URBAN HEAT ISLAND INTENSITY IN URBAN CITIES USING MODIS SATELLITE DATA. *ISPRS Archives, 2019, XLII-4/W16. 6th (GGT 2019)*, 1–3 October **2019**, Kuala Lumpur, Malaysia.

Frey, C.M.; Rigo, G.; Parlow, E. Investigation of the daily Urban Cooling Island (UCI) in two coastal cities in an arid environment: Dubai and Abu Dhabi (UAE). *City 81*, **2012**, p. 2.06.

Lazzarini, M.; Marpu, P.R.; Ghedira, H. Temperature-land cover interactions: The inversion of urban heat island phenomenon in desert city areas. *Remote Sens. Environ*. **2013**, 130, 136–152.

Cai, G.; Du, M. Relationship between thermal inertia and urban heat sink in Beijing derived from Satellite images. *JURSE*. **2009**, Shanghai, pp. 1-5, doi: 10.1109/URS.2009.5137495.

Li, S.; Mo, H.; Dai, Y. Spatio-temporal pattern of Urban Cool Island Intensity and its eco-environmental response in Chang-Zhu-Tan Urban Agglomeration. *Commun. Inf. Sci. Manage. Eng.* **2011**.

Steeneveld, G. J.; Koopmans, S.; Heusinkveld, B. G.; van Hove, L. W. A.; Holtslag, A. A. M. Quantifying urban heat island effects and human comfort for cities of variable size and urban morphology in the Netherlands. *J. Geophys. Res*. **2011**, 116, D20129, doi:10.1029/2011JD015988.

Oke T R. The energetic basis of the urban heat island. *Q. J. R. Meteorol. Soc.* **1982**, 108 1–24

Gago, E.; Berrizbeitia, S.; Torres, R.; Muneer, T. Effect of Land Use/Cover Changes on Urban Cool Island Phenomenon in Seville, Spain. *Energies* **2020**, *13*, 3040.

Rotach M W et al .BUBBLE—an urban boundary layer meteorology project. *Theor. Appl. Climatol.* **2005**, 81 231–61, 10.1007/s00704-004-0117-9.

Imhoff, M. L.; Zhang, P.; Wolfe, R. E.; Bounoua, L. Remote sensing of the urban heat island effect across biomes in the continental USA. *Remote Sens. Environ.* **2010**, 114 504–13

Georgescu, M.; Moustaoui, M.; Mahalov, A.; Dudhia, J. An alternative explanation of the semiarid urban area oasis effect. *J. Geophys. Res. Atmos*. **2011**, 116 D24

Gedzelman, S.D.; Austin, S.; Cermak, R.; Stefano, N.; Partridge, S.; Quesenberry, S.; Robinson, D.A. Mesoscale aspects of the Urban Heat Island around New York City. *Theor. Appl. Climatol*. **2003**, 75, 29–42.

Campbell, J.B. Introduction to Remote Sensing, 3rd ed.; *The Guilford Press:* New York, NY, USA, 2002. 111. Sandholt, I.; Rasmussen, K.; Andersen, J. A simple interpretation of the surface temperature/vegetation index space for assessment of surface moisture status. Remote Sens. Environ. **2002**, 79, 213–224.

Sandholt, I.; Rasmussen, K.; Andersen, J. A simple interpretation of the surface temperature/vegetation index space for assessment of surface moisture status. *Remote Sens. Environ*. **2002**, 79, 213–224.

Carnahan, W.H.; Larson, R.C. An analysis of an urban heat sink. *Remote Sens. Environ*. **1990**, 33, 65–71.

Larson, R.C.; Carnahan,W.H. The influence of surface characteristics on urban radiant temperatures. *Geocarto Int.* **1997**, 12, 5–16.

Stewart, I.; Oke, T. Newly developed “thermal climate zones” for defining and measuring urban heat island magnitude in the canopy layer. *In Proceedings of the T.R. Oke Symposium: Urban Scales, Urban Systems and the Urban Heat Island (Joint between the Timothy R. Oke Symposium and the Eighth Symposium on the Urban Environment),* Garmisch-Partenkirchen, Germany, 12 January **2009**.

Rasul, A.; Balzter, H.; Smith, C.; Remedios, J.; Adamu, B.; Sobrino, J.A.; Srivanit, M.; Weng, Q. A Review on Remote Sensing of Urban Heat and Cool Islands. *Land*, **2017**, 6, 38. https://doi.org/10.3390/land6020038

Essa, W.; Verbeiren, B.; van der Kwast, J.; Batelaan, O. Evaluation of DisTrad thermal sharpening for urban areas. *INT J APPL EARTH OBS*. **2012**, 19, 63-172. https://doi.org/10.1016/j.jag.2012.05.010.

Chen, X.; Zhao, H.; Li, P.; Yin, Z. 2006. Remote sensing image-based analysis of the relationship between urban heat island and land use/cover changes. *Remote Sens. Environ*. **2006**, 104, 133–146.

Schwarz, N.; Lautenbach, S.; Seppelt, R. Exploring indicators for quantifying surface urban heat islands of European cities with MODIS land surface

temperatures. *Remote Sens. Environ.* **2011**, 115, 3175–3186.

Firozjaei, M.K.; Sedighi, A.; Argany, M.; Jelokhani-Niaraki, M.; Arsanjani, J.J. A geographical direction-based approach for capturing the local variation of urban expansion in the application of ca-markov model. *Cities*, **2019**, 93, 120–135.

Sun, Zhongchang.; Wang, Cuizhen.; Guo, Qing.; Shang, Ranran. A Modified Normalized Difference Impervious Surface Index (MNDISI) for Automatic Urban Mapping from Landsat Imagery. *Remote Sens*. **2017**, 9. 942. DOI:10.3390/rs9090942

Essa, W.; Verbeiren, B.; van der Kwast, J.; Batelaan, O. Improved DisTrad for downscaling thermal MODIS imagery over urban areas. *Remote Sens.* **2017**, 8, 1243–1250. https://doi.org/10.3390/rs9121243.

Clinton, N.; Gong, P., (2013). MODIS detected surface urban heat islands and sinks: Global locations and controls. *Remote Sens. Environ*. **2013**, 134: 294-304 (11 pages).

Yi, Zhou.; Guang, Yang.; Shixin, Wang.; Litao, Wang.; Futao, Wang.; Xiongfei, Liu. A new index for mapping built-up and bare land areas from Landsat-8 OLI data, *Remote Sens Lett.* **2014**, 5:10, 862-871, DOI: 10.1080/2150704X.2014.973996

Zhao, H. M.; X. L. Chen. Use of Normalized Difference Bareness Index in Quickly Mapping Bare Areas from TM/ETM.": *IEEE IGARSS,* **2005**, Seoul, South Korea. url: <Goto ISI>://WOS:000237237602044

Kustas, W.; Norman, J.; Anderson, M.; French, A. Estimating sub-pixel surface temperatures and energy fluxes from the vegetation index–radiometric temperature relationship. *Remote Sens. Environ*. **2003**, 85:429–440. https://doi.org/10.1016/S0034-4257(03)00036-1.

Sun, G.Y.; Chen, X.L.; Jia, X.P.; Yao, Y.J.; Wang, Z.J. Combinational build-up index (CBI) for effective impervious surface mapping in urban areas. *IEEE J. Sel. Top. Appl. Earth Obs. Remote Sens*. **2016**, 9, 2081–2092. https://dx.doi.org/10.1109/JSTARS.2015.2478914

Deng, C.; Wu, C. BCI: A biophysical composition index for remote sensing of urban environments. *Remote Sens. Environ*. **2012**, 127, 247–259.

Rasul, A.; Balzter, H.; Ibrahim, G.R.F.; Hameed, H.M.; Wheeler, J.; Adamu, B.; Ibrahim, S.; Najmaddin, P.M. Applying Built-Up and Bare-Soil Indices from Landsat 8 to Cities in Dry Climates. *Land***, 2018**, 7, 81. doi:10.3390/land7030081

PHG for Water and Environ Resour Dev. Quality use of home reverse osmosis filters of some areas in Gaza Strip, **2002**.

Essa, W.; Lhissou, R. Evaluating Built-up Indices for DisTrad Thermal Sharpening over the Arid and Semi-Arid Regions; Case Study: Gaza Strip. LIEGE (BELGIUM) Earth Observation for sustainable cities and communities, *6th EARSel Joint Workshop Urban remote Sensing.* **2021**, 26 – 28 MAY 2021. Liege, Belgium.

Congedo, L. Semi-Automatic Classification Plugin documentation. *Release.* **2016**, 225–235. DOI: 10.13140/RG.2.2.29474.02242/1

Mallick, J.; Singh, C. K.; Shashtri, S.; Rahman, A.; Mukherjee, S. Land surface emissivity retrieval based on moisture index from LANDSAT TM satellite data over heterogeneous surfaces of Delhi city. *Int J Appl Earth Obs Geoinf*, **2012**, 19, 348 - 358

Bouzekri, S.; Lasbet, A.A.; Lachehab, A. A new spectral index for extraction of built-up area using landsat-8 data*. J. Indian Soc. Remote Sens*. **2015**, 43, 867–873.

Waqar, M.M.; Mirza, J.F.; Mumtaz, R.; Hussain, E. Development of new indices for extraction of built-up area & bare soil from landsat data. *Open Access Sci. Rep*. **2012**, 1, 4.

Roy, P.; Miyatake, S.; Rikimaru, A. Biophysical Spectral Response Modeling Approach for Forest Density Stratification. Available online: http://www.gisdelopment.net/aars/acrs/1997/tTM5/tTM5008a.shtml (accessed on 22 July 2018).

He, C.; Shi, P.; Xie, D.; Zhao, Y. Improving the normalized difference built-up index to map urban built-up areas using a semiautomatic segmentation approach. *Remote Sens. Lett.* ***2010,*** 1, 213–221.

Zuraini, B.; Nor, A. IMPERVIOUS SURFACE DETECTION AND MAPPING VIA DIGITAL REMOTELY SENSED TECHNIQUES. *Int. Conf. CBEE.* **2014**, May 27-28, Istanbul (Turkey).

Xu, H. A New Index for Delineating Built-Up Land Features in Satellite Imagery. *Int. J. Remote Sens.* **2008**, 29: 4269–4276. doi:10.1080/01431160802039957.

Carlson, T.N.; Arthur, S.T. The impact of land use — land cover changes due to urbanization on surface microclimate and hydrology: a satellite perspective. *Glob Planet Change*, **2000**, 25,1–2:49-65, ISSN 0921-8181, https://doi.org/10.1016/S0921-8181(00)00021-7.

Bhatti, S.S.; Tripathi, N.K. Built-up area extraction using Landsat 8 OLI imagery. *GISci. Remote Sens.* **2014**, 51, 445–467.

Jieli, C.; Manchun, L.; Yongxue, L.; Chenglei, S. Extract residential areas automatically by New Built-up Index. *Int. Conf. – CPGIS.* **2010**, pp. 1–5.

Priyakant, S.; Niva, V.; Eskindir, A. Urban Built-up Area Extraction and Change Detection of Adama Municipal Area using Time-Series Landsat Images. *Int. J. Adv. Remote Sens. and GIS*. **2016**. 1886-1895. 10.23953/cloud.ijarsg.67.

Zha, Y.; Gao, J.; Ni, S. Use of normalized difference built-up index in automatically mapping urban areas from TM imagery. *Int. J. Remote Sens.* **2003**, 24, 583–594.

Rogers, A.; Kearney, M. Reducing signature variability in unmixing coastal marsh Thematic Mapper scenes using spectral indices. *Int. J. Remote Sens.* **2004**, 25, 2317–2335.

Van de Griend, A.; Owe, M. On the relationship between thermal emissivity and the normalized different vegetation index for natural surfaces. *Int. J. Remote Sens*. **1993**, 14, 1119–1131.

Huete, A.R. A Soil-Adjusted Vegetation Index (SAVI). *Remote Sens. Environ*. **1988**, 25 (3), 295-309.

Kawamura, M.; Jayamana, S.; Tsujiko, Y. Relation between social and environmental conditions in Colombo Sri Lanka and the urban index estimated by satellite remote sensing data. *Int. Arch. Photogramm. Remote Sens.* **1996**, 31, 321–326. https://ci.nii.ac.jp/naid/10003189515/

Estoque, R.; Murayama, Y. Classification and change detection of built-up lands from Landsat-7 ETM+ and Landsat-8 OLI/TIRS imageries: A comparative assessment of various spectral indices. *Ecol. Indic.* **2015**, 56. 10.1016/j.ecolind.2015.03.037.

Stathakis, D.; Perakis, K.; Savin, I. Efficient segmentation of urban areas by the VIBI. *Int. J. Remote Sens.* **2012**, 33, 6361–6377.

Kohonen T," Self-Organizing Maps " 3rd edition, Springer, Berlin, 2001

Qi, J.; Chehbouni, A.; Huete, A.R.; Kerr, Y.H.; Sorooshian, S. A modified soil adjusted vegetation index. *Remote Sens. Environ.* **1994**, 48, 119–126 (1994). doi:10.1016/0034-4257(94) 90134-1

Bhatt, a.; Ghosh S.K., Kumar, K. Spectral Indices Based Change Detection in an Urban Area Using Landsat Data. In: Pant M., Deep K., Bansal J., Nagar A., Das K. (eds) *Proceedings of Fifth International Conference on Soft Computing for Problem Solving. Advances in Intelligent Systems and Computing,* ***2016****, 437. Springer, Singapore.* https://doi.org/10.1007/978-981-10-0451-3_39

Bramhe, V. S.; Ghosh, S. K.; Garg, P. K. EXTRACTION OF BUILT-UP AREA BY COMBINING TEXTURAL FEATURES AND SPECTRAL INDICES FROM LANDSAT-8 MULTISPECTRAL IMAGE. *ISPRS - Int. Arch. Photogramm. Remote Sens. Spatial Inf. Sci., XLII-5*, **2018**, 727–733. https://doi.org/10.5194/isprs-archives-XLII-5-727-2018

Firozjaei, M.K.; Sedighi, A.; Kiavarz, M.; Qureshi, S.; Haase, D.; Alavipanah, S.K. Automated Built-Up Extraction Index: A New Technique for Mapping Surface Built-Up Areas Using LANDSAT 8 OLI Imagery. *Remote Sens.* **2019**, 11, 1966.

Nandy, S.; Joshi, P.K.; Das, K.K. Forest canopy density stratification using biophysical modeling. *J Indian Soc Remote Sens*. **2003**, 31, 291–297 (2003). https://doi.org/10.1007/BF03007349

T. Owen, W.; Carlson, T. N.; Gillies, R. R. An assessment of satellite remotely-sensed land cover parameters in quantitatively describing the climatic effect of urbanization, *Int. J. Remote Sens*. **1998**, 19:9, 1663-1681 To link to this article: http://dx.doi.org/10.1080/014311698215171

Li, H.; Zhou, Y.; Li, X.; Meng, L.; Wang, X.; Wu, S.; Sodoudi, S. A new method to quantify surface urban heat island intensity. *Sci. Total Environ*. **2018**, 624, 262–272.

Congedo, Luca. Semi-Automatic Classification Plugin: A Python tool for the download and processing of remote sensing images in QGIS. *Journal of Open Source Software,* **2021***,* 6(64), 3172, https://doi.org/10.21105/joss.03172.